JMEPEG (2016) 25:510–517
DOI: 10.1007/s11665-016-1883-0

1059-9495/$19.00

The Corrosion Behavior of $Ni_3(Si,Nb)$ Alloys in Boiling 70 wt.% Sulfuric Acid

Jen-Hsien Hsu, Christopher M. Larson, Joseph W. Newkirk, Richard K. Brow, and San-Hong Zhang

(Submitted July 23, 2015; in revised form November 23, 2015; published online January 12, 2016)

Corrosion-resistant $Ni_3(Si,Nb)$ alloys are promising materials of construction for hydrogen-production systems based on the sulfur-iodine thermochemical cycle. In this work, the corrosion rates of three different $Ni_3(Si,Nb)$ alloys were measured in boiling 70 wt.% sulfuric acid and a three-stage corrosion mechanism was identified, based on the composition and morphology of surface scale that developed. The α(Ni) + β(Ni_3Si) eutectic constituent of the alloy microstructure was selectively attacked by acid and, when present, is detrimental to corrosion resistance. The G-phase ($Ni_{16}Si_{17}Nb_6$) is more passive than the β-matrix and seems to contribute to a lower steady-state corrosion rate.

Keywords corrosion, Ni-Si alloys, sulfur-iodine cycle, sulfuric acid

1. Introduction

The sulfur-iodine thermochemical cycle (S-I cycle) has been proposed to produce large volumes of hydrogen from water. The S-I cycle is a closed-loop system that produces no byproducts other than H_2 and O_2 and is suitable with different heat sources, including solar and nuclear (Ref 1, 2). However, the very corrosive operating conditions, e.g., high temperatures (up to 850 °C) and 50 to 98 wt.% boiling sulfuric acid, limit the possible materials of construction. In addition to precious metals (like Pt) and very brittle alloys like Fe-14Si (UNS 47003) (Ref 3), more ductile, corrosion-resistant $Ni_3(Si,Nb)$-based alloys are candidate construction materials for the S-I cycle systems (Ref 4, 5). $Ni_3(Si,Nb)$-based alloys also retain 50% of their room temperature strength at 900 °C and have been successfully joined using tungsten inert welding techniques (Ref 5, 6).

Ni_3Si intermetallic alloys are known to resist corrosive attack by sulfuric acids. As-cast Ni-10Si-3Cu alloy (Hastelloy D^2) has good corrosion resistance to all concentrations of boiling sulfuric acid, with corrosion rates of 0.5 mm $year^{-1}$ (20 mpy) in 60 wt.% H_2SO_4 and 2 mm $year^{-1}$ (80 mpy) in 77 wt.% H_2SO_4 (Ref 4, 7). However, as-cast Ni-10Si-3Cu alloy is brittle, as indicated by its zero elongation in room temperature tensile tests (Ref 7). Removing the brittle Ni_5Si_2 (γ) phase by heat treatment increases the corrosion rate in 60 wt.% H_2SO_4 of heat-treated Ni-10Si-3Cu alloy to >20.3 mm $year^{-1}$ (800 mpy) due to the formation of a secondary β-phase (Ref 8). $Ni_3(Si,Ti)$ alloys (single β-phase) can achieve ~30% ductility at room temperature and have excellent corrosion resistance (<0.13 mm $year^{-1}$ (5 mpy)) to boiling concentrated (80 and 94 wt.%) sulfuric acid (Ref 7, 9). However, the steady-state corrosion rate of $Ni_3(Si,Ti)$ alloys is >1.5 mm $year^{-1}$ (60 mpy) in 26-70 wt.% boiling sulfuric acid (Ref 6, 7, 10).

The microstructures of the as-cast $Ni_3(Si,Nb)$ alloys can include the α(Ni) + β(Ni_3Si) eutectic, β-(Ni_3Si), G-($Ni_{16}Si_{17}Nb_6$), and γ-phases (Ni_5Si_2), depending on composition (Ref 5, 11). Among those phases, γ- phase and G-phase are brittle, and α + β eutectic seems to be susceptible to sulfuric acid corrosion (Ref 6). Newkirk et al. developed $Ni_3(Si,Nb)$ alloys that, with the proper heat treatment conditions and control of the Nb content, have improved ductility (Ref 5, 12). After a homogenization heat treatment at 950 °C for 4 days, the brittle γ-phase dissolved into the β-matrix. By controlling Nb content close to the solubility limit (1.2 at.%) in β-matrix and the total Si + Nb content to the range 22 to 24.5 at.%, the fraction of α + β eutectic and G-phase can be significantly reduced. The homogenized $Ni_3(Si,Nb)$ alloys without α + β eutectic (<1% area fraction) can be deformed more than 50% by multiple cold rolling passes and have steady-state corrosion rates <0.13 mm $year^{-1}$ (5 mpy) in boiling 70 wt.% sulfuric acid (Ref 5). However, the effect of the G-phase content on the corrosion rate and the effect of α + β eutectic on corrosion are not clear. Further, Larson measured weight changes of $Ni_3(Si,Ti,Nb)$ alloys exposed to boiling 70 wt.% sulfuric acid and found evidence for a multi-step corrosion process without developing a mechanism (Ref 10).

The corrosive nature of sulfuric acid strongly depends on its concentration and temperature (Ref 13, 14). Sulfuric acid concentrations up to 65 wt.%, are reducing at all temperatures. For concentrations in the range of 65-85 wt.%, sulfuric acids are reducing at room temperature, but are oxidizing at their boiling temperature (Ref 14). Evans et al. reported that the corrosion mechanism of an as-cast Ni_3Si-based alloy (with 9.7 at.% Si, 2.5 at.% Ti, 2 at.% Cu and 2.8 at.% Mo) differs in three distinct concentration ranges of sulfuric acids at their boiling points, and that the corrosion rate is greatest within the intermediate concentration range (47-55 wt.%) (Ref 15). Earlier work in our lab also showed that 70 wt.% sulfuric acid aggressively attacked $Ni_3(Si,Nb)$ alloys (Ref 6, 10).

Jen-Hsien Hsu, Christopher M. Larson, Joseph W. Newkirk, Richard K. Brow, and **San-Hong Zhang,** Department of Material Science and Engineering, Missouri University of Science and Technology, 282 McNutt Hall, 1400 N. Bishop, Rolla, MO 65409-0330, USA. Contact e-mails: jhy27@mst.edu and jnewkirk@mst.edu.

In this paper, the corrosion behavior of three $Ni_3(Si,Nb)$ alloys in boiling 70 wt.% sulfuric acid is described. Weight changes with corrosion time were recorded and related to the development of the surface scale. The influence of the α + β eutectic and the G-phase, which cannot be removed by heat treatment, on corrosion is discussed.

2. Experimental Procedures

2.1 Preparation of $Ni_3(Si,Nb)$ Alloys

Three $Ni_3(Si,Nb)$ alloys, with the nominal compositions $NiSi_{18}Nb_5B_{0.5}$, $NiSi_{20}Nb_3B_{0.5}$, and $NiSi_{21}Nb_{1.6}B_{0.5}$ were prepared for this work. Boron (0.5 at.%) was added to reduce moisture-induced hydrogen embrittlement and so to improve room temperature ductility in air (Ref 16). The alloys were melted at 1500 °C in an induction furnace under an argon atmosphere and held about 15 min for homogenization. The melt temperature was lowered to 1350 °C and held about 5 min before casting. The nominal and analyzed compositions, based on spark emission spectrometry, of the alloys are shown in Table 1 (Ref 6).

2.2 Corrosion Tests

The corrosion tests are based on ASTM G31-72 (Ref 17). The 70 wt.% sulfuric acid was heated in a Pyrex flask on a hot plate to its boiling point (~165 °C at 1 atm) (Ref 18); the temperature of the sulfuric acid was monitored by a thermometer. As the boiling temperature is dependent on the concentration, monitoring the temperature provided a check on concentration. A water-cooled condenser was used to cool the acid vapor and return the liquid back to the flask.

Test coupons, 10 mm × 7 mm × 3 mm, were cut from homogenized alloy ingots with a diamond blade, ground by #1200 SiC paper, cleaned by acetone, and weighed. The coupons were tied with Teflon string, then immersed in 400 mL of boiling 70 wt.% sulfuric acid. After each immersion for a fixed time, the coupons were rinsed with water, air-dried, and then re-weighed. Fresh 70 wt.% sulfuric acid was used for every new set of corrosion tests. At least two coupons were tested for each set of experimental conditions.

The surface compositions of corroded samples were obtained using scanning Auger electron spectroscopy (Physical Electronics Phi-680 scanning Auger nanoprobe). Depth profiling was performed in selected areas by monitoring the Auger signal of selected elements while alternately sputtering with an argon ion beam for a given amount of time.

Microstructural and compositional characterization of the surfaces and cross sections of the corroded $Ni_3(Si,Nb)$ alloys were done by scanning electron microscopy (Hitachi S570 SEM) with energy dispersive spectroscopy (EDS), and by x-ray diffraction (Philips X-Pert Diffractometer). The specimens were prepared using normal metallography procedures.

3. Results and Discussion

Figure 1 shows that the microstructure of the homogenized $NiSi_{18}Nb_5B_{0.5}$ alloy has a significant fraction of α + β eutectic and the G-phase, in addition to the β-matrix phase; $NiSi_{20}Nb_3B_{0.5}$ has less G-phase and almost no α + β eutectic; $NiSi_{21}Nb_{1.6}B_{0.5}$ has the least amount of G-phase and a little of α + β eutectic. The microstructures of all alloys were analyzed using the Image J 1.45s software package and the quantitative results are summarized in Table 1. The details of alloy casting and heat treatments, and their effects on microstructure are reported in Ref 5 and 6.

3.1 Weight Loss in Corrosion Tests

Figure 2(a) shows the weight loss results for the three $Ni_3(Si,Nb)$ alloys in boiling 70 wt.% sulfuric acid. The weight losses were normalized to the initial geometric surface area of each coupon. The weight loss rates for all three alloys decrease after an initial induction period. The long-term weight loss rate for the $NiSi_{18}Nb_5B_{0.5}$ coupons is at least seven times faster than those for the other two alloys. Weight changes arise from both the dissolution of alloy components, principally Ni (Ref 10), and the formation of an oxide scale, described below. The overall dissolution weight loss is about five times greater than the overall weight gained by scale formation (Appendix).

The apparent passivation of Ni-Si alloys exposed to concentrated sulfuric acid has been reported previously. In boiling sulfuric acid from 5 to 95 wt.%, the polarization curves of $Ni_3(Si,Ti,Cu)$ alloys showed an active region, an active-to-passive transition, a passive range and finally a passive-to-transpassive transition (Ref 15, 19). $Ni_3(Si,Nb)$ alloys also showed the typical active-passive-transpassive curve in 70 wt.% sulfuric acid at room temperature (Ref 6).

The weight loss versus corrosion time data in Fig. 2(a) were replotted on log-log scales in Fig. 2(b), which reveals three linear regions with slopes of ~0.4, ~1 and ~0.01 (~0.1 for $NiSi_{18}Nb_5B_{0.5}$), respectively. These three regions are designated as corrosion Stages I, II, and III. Stage I typically lasts for less

Table 1 Alloy compositions (in wt.%), microstructural analysis, and corrosion results (Ref 6)

		Composition				Area fraction, %		Corrosion results	
Alloys		Ni	Si	Nb	B	G-phase	α + β eutectic	(steady-state) Corrosion rate, mm year^{-1}	Passivation time, min
$NiSi_{18}Nb_5B_{0.5}$	N[A]	82.2	9.3	8.6	0.1	16 ± 1.5	27 ± 3	1.00 ± 0.19	330 ± 61
	A[B]	…	…	…	…				
$NiSi_{20}Nb_3B_{0.5}$	N[A]	84.2	10.5	5.2	0.1	8 ± 0.4	~0	0.03 ± 0.005	480 ± 41
	A[B]	84.4	10.3	5.3	0.04				
$NiSi_{21}Nb_{1.6}B_{0.5}$	N[A]	86.3	11.5	2.8	0.1	1.4 ± 0.5	1 ± 0.2	0.15 ± 0.03	430 ± 26
	A[B]	86.1	10.9	2.9	0.1				

[A] Nominal composition; [B] analysis results of spark optical emission spectrometry

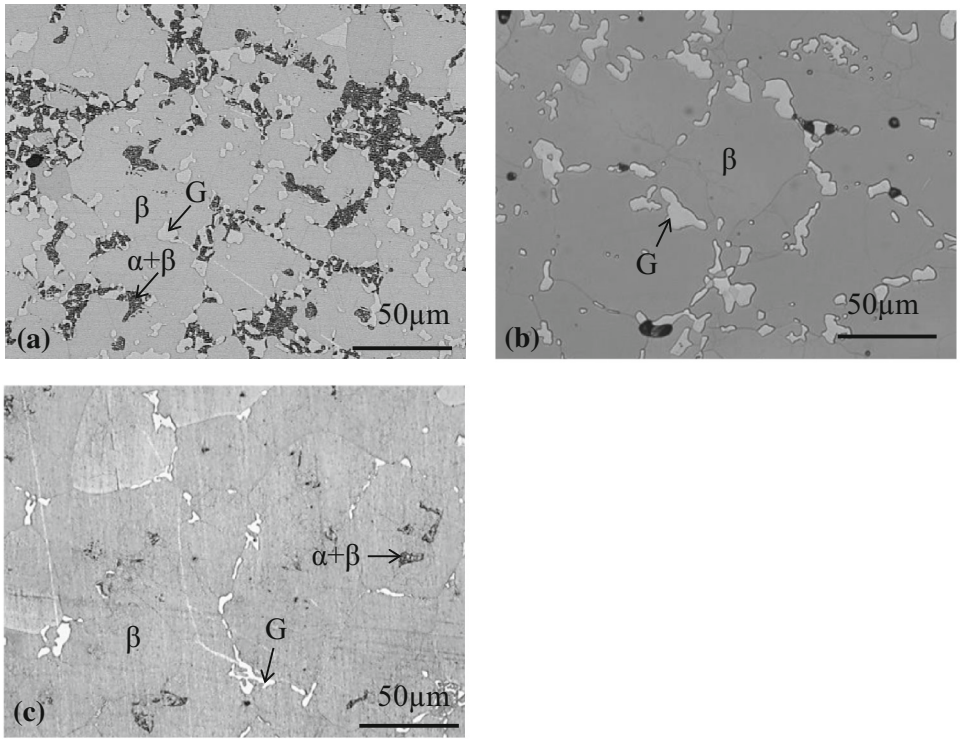

Fig. 1 Microstructures of (a) $NiSi_{18}Nb_5B_{0.5}$ (b) $NiSi_{20}Nb_3B_{0.5}$ (c) $NiSi_{21}Nb_{1.6}B_{0.5}$ after the 4-day homogenization heat treatment at 950 °C

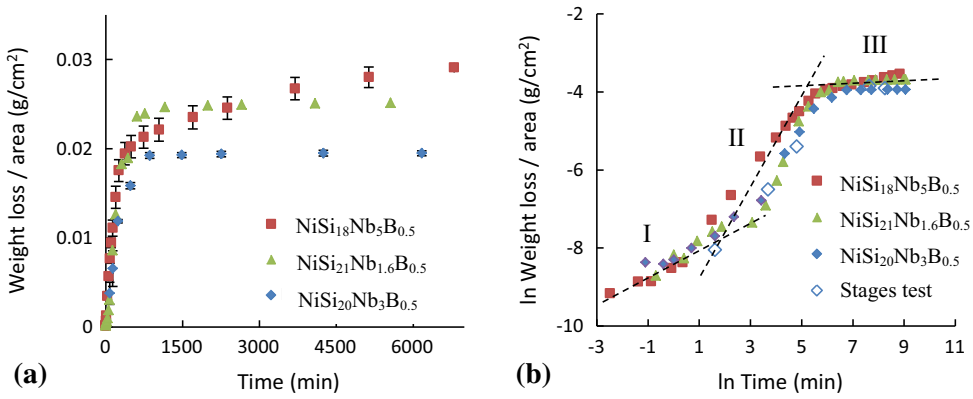

Fig. 2 (a) The normalized weight loss and (b) its natural logarithm for $Ni_3(Si,Nb)$ alloys in boiling 70 wt.% sulfuric acid

than 20 min and the overall weight loss is minor (< 1% of the overall change in weight). Stage II lasts for hundreds of minutes and is the stage where most (> 90%) of the weight lost occurs. Stage III indicates alloy passivation and has the lowest weight-loss rate. In this paper, the passivation time is defined as the onset of Stage III and the steady-state corrosion rate is calculated from the long-term, Stage III weight loss rate; passivation times and steady-state corrosion rates for the three alloys are given in Table 1. The $NiSi_{20}Nb_3B_{0.5}$ and $NiSi_{21}Nb_{1.6}B_{0.5}$ alloys exhibit corrosion rates (~0.03 and 0.15 mm year^{-1} (1.2 and 6 mpy), respectively) that are much lower than that for the $NiSi_{18}Nb_5B_{0.5}$ alloy (~1 mm year^{-1} (39 mpy). With these measured corrosion rates, the current densities of $NiSi_{18}Nb_5B_{0.5}$ (82 μA cm^{-2}), $NiSi_{20}Nb_3B_{0.5}$ (2.6 μA cm^{-2}), and $NiSi_{21}Nb_{1.6}B_{0.5}$ (13 μA cm^{-2}) in Stage III, estimated using Faraday's law (Ref 24), show two orders of magnitudes difference to the passivation current density (100-400 μA cm^{-2}) in the anodic polarization curves in 70 wt.% sulfuric acid at room temperature for $Ni_3(Si,Nb)$ alloys (Ref 6). The passivation current density might be even larger at the boiling point of 70 wt.% sulfuric acid (Ref 20). Similar conditions were happened to Evans et al. results (Ref 15). They reported that the Ni_3Si-based alloy passivated spontaneously in the boiling sulfuric acid > 55 wt.%, and the passivation current density (~100 μA cm^{-2}) in the anodic polarization curves in boiling 75 wt.% sulfuric acid was also two orders of magnitudes larger than that (~3 μA cm^{-2}), based on the measured corrosion rate. So, the corrosion mechanism of Ni_3Si-based alloy might not be fully interpreted by the simple equation of Faraday's law and the three alloys in this report still might passivate in Stage III.

3.2 Compositional and Microstructural Analyses

Five fresh coupons of each alloy were exposed to boiling 70 wt.% sulfuric acid for different times, then removed, rinsed in water, weighed, and then analyzed by analytical scanning electron microscopy. The corrosion times were selected so that one sample represented Stage I conditions, and two each represented Stages II and III. The weight losses measured from these individual samples corresponded with those from the continuous tests. For example, the weight loss rates from the five $NiSi_{20}Nb_3B_{0.5}$ coupons are plotted as the open symbols in Fig. 2(b).

3.2.1 Surface Morphology. Figure 3 shows the representative surface morphologies of $NiSi_{20}Nb_3B_{0.5}$ coupons removed from boiling 70 wt.% sulfuric acid after the three corrosion stages. EDS-mapping of the Stage I (5 min) surface (Fig. 3a) shows the presence of islands of a silica-rich phase. In Stage II (122 min) a continuous oxide film has covered the entire surface. In Stage III (63 h), a topologically rough oxide film has formed (Fig. 3c). White particles that were suspended in the acid at the end of the corrosion experiments were collected and analyzed by EDS, and were found to have similar compositions to the silica-rich surface oxides (Table 2). The surface scale compositions and morphologies of the other two alloys, $NiSi_{18}Nb_5B_{0.5}$ and $NiSi_{21}Nb_{1.6}B_{0.5}$, evolved in a similar manner, and those compositions are also reported in Table 2.

3.2.2 Cross-sectional Analyses. Figure 4 shows examples of cross-sectional micrographs of corroded $NiSi_{20}Nb_3B_{0.5}$ after the different corrosion stages. (The Cr layer present in these micrographs was deposited on the sample surface prior to normal metallographic preparation procedures.) There is no evidence for enhanced corrosion along grain boundaries, nor is there evidence from EDS-mapping (not shown) and back-scattered electron images for the formation of secondary phases in the oxide layer. The stoichiometry (by EDS) of the oxide scales that formed on each sample during all three corrosion stages is close to SiO_2 (Table 2). Other than a slightly greater nickel content in the oxide scales at Stage I and Stage II (Table 2), no significant compositional or structural differences between the stages were observed. It is unclear if the cracks that are observed in the oxide scales were original or caused by the metallographic preparation procedures.

For the corroded $NiSi_{18}Nb_5B_{0.5}$ coupons, significant internal penetration occurred along the $\alpha + \beta$ eutectic. From EDS-mapping of the cross sections (Fig. 5b), the oxygen signals associated with silicon signals penetrate the metal along the $\alpha + \beta$ eutectic. The penetration front can also be clearly recognized in the associated micrograph (Fig. 5a). Evans et al. (Ref 7) and Zhang (Ref 6) also reported that the α-phase and the $\alpha + \beta$ eutectic were preferentially oxidized by boiling concentrated sulfuric acid. This might be the major reason that the steady-state corrosion rate of the $NiSi_{18}Nb_5B_{0.5}$ alloy is greater than the other two $Ni_3(Si,Nb)$ alloys (Fig. 2).

The cross-sectional micrographs were used to measure the thickness of the oxide layers on the corroded alloys (Fig. 6a). For all alloys, the oxide thickness increases with exposure time before Stage III, and then seems to stop. However, the depth of internal penetration along the $\alpha + \beta$ eutectic of the $NiSi_{18}Nb_5B_{0.5}$ samples continues to increase with corrosion time, even in Stage III. On a log-log plot (Fig. 6b), the slopes of the time dependence of the oxide thickness (before passivation)

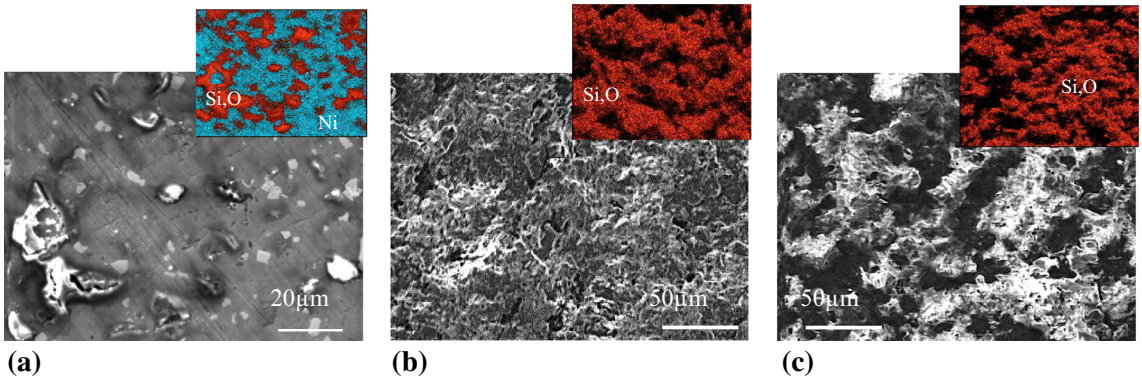

Fig. 3 Surface morphology and EDS-maps for $NiSi_{20}Nb_3B_{0.5}$ after exposure to boiling 70 wt.% sulfuric acid: (a) 5 min (Stage I); (b) 122 min (Stage II); (c) 63 h (Stage III)

Table 2 Chemical composition (by EDS; in at.%) of the surface scale that forms on $Ni_3(Si,Nb)$ alloys in boiling 70 wt.% sulfuric acid

	$NiSi_{18}Nb_5B_{0.5}$			$NiSi_{20}Nb_3B_{0.5}$				$NiSi_{21}Nb_{1.6}B_{0.5}$		
	Stage I (1 min)	Stage II (125 min)	Stage III (63 h)	Suspension	Stage I (5 min)	Stage II (122 min)	Stage III (63 h)	Stage I (3 min)	Stage II (50 min)	Stage III (63 h)
Si	26.6 ± 0.8	30.3 ± 0.4	31.9 ± 0.2	30.6 ± 0.7	27.3 ± 0.9	30.4 ± 0.9	30.4 ± 0.1	32.7 ± 0.5	29.3 ± 0.8	31.0 ± 0.1
S	1.4 ± 0.3	1.9 ± 0.2	0.9 ± 0.2	1.2 ± 0.2	1.2 ± 0.2	1.0 ± 0.1	2.1 ± 0.1	1.8 ± 0.2	1.7 ± 0.7	1.5 ± 0.1
Ni	3.1 ± 0.6	0.9 ± 0.1	0.5 ± 0.2	…	2.8 ± 0.3	2.0 ± 0.7	0.4 ± 0.1	3.1 ± 0.4	2.7 ± 0.4	0.5 ± 0.1
O	68.9 ± 0.9	67.0 ± 0.1	66.8 ± 0.1	69.1 ± 0.3	68.7 ± 0.8	66.4 ± 0.2	67.3 ± 0.1	62.4 ± 1.8	66.4 ± 0.3	67.0 ± 0.1

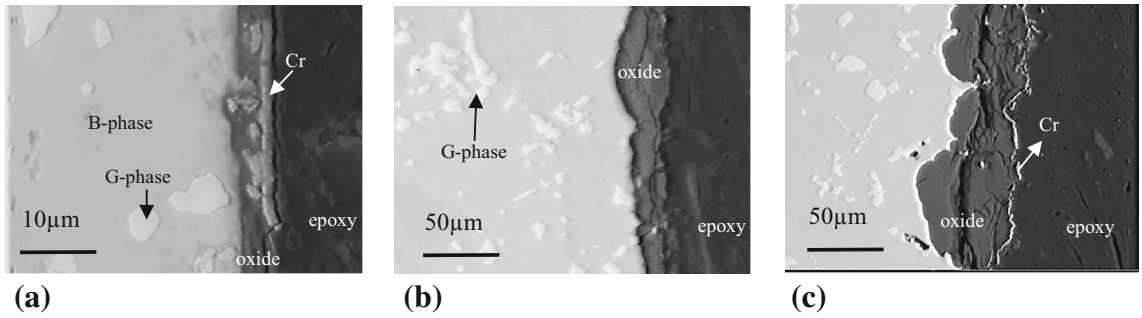

Fig. 4 Cross section of $NiSi_{20}Nb_3B_{0.5}$ coupons after exposure to boiling 70 wt.% sulfuric acid: (a) 5 min (Stage I); (b) 122 min (Stage II); (c) 63 h (Stage III)

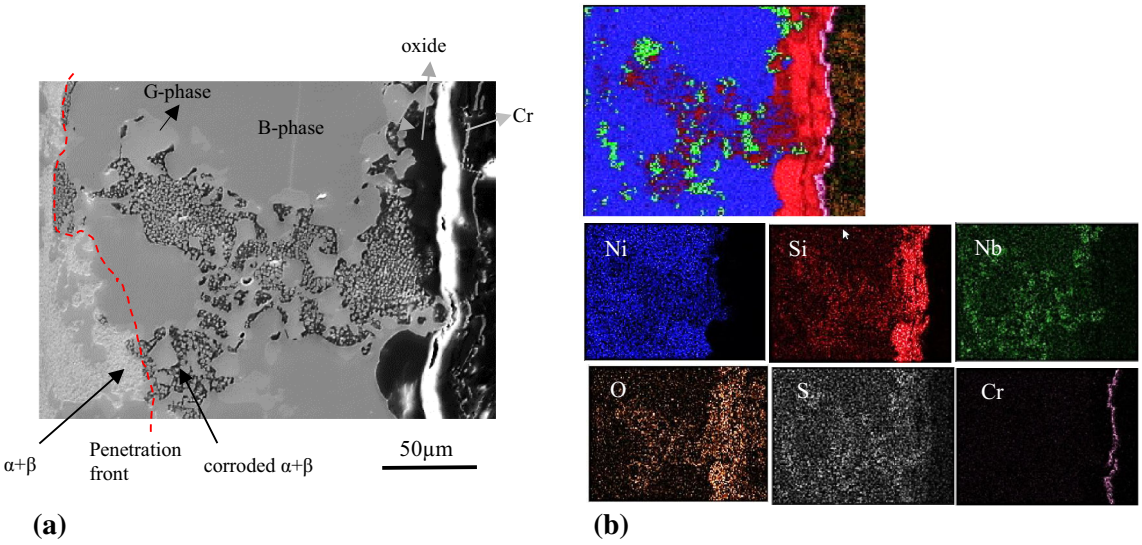

Fig. 5 (a) Micrograph and (b) EDS-maps of a cross section of $NiSi_{18}Nb_5B_{0.5}$ after 63 h (Stage III) exposure to boiling 70 wt.% sulfuric acid

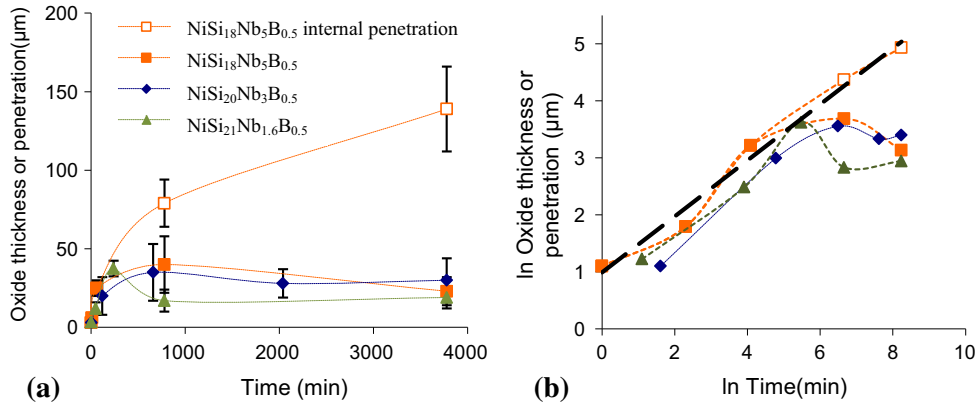

Fig. 6 (a) Oxide thickness of the Ni_3Si alloys (and internal penetration depth of $NiSi_{18}Nb_5B_{0.5}$) with exposure time to boiling 70 wt.% sulfuric acid; (b) the natural logarithm of the oxide thickness (or penetration depth) with exposure time. The dashed line has a slope of 0.5

and the depth of internal penetration of the $NiSi_{18}Nb_5B_{0.5}$ samples are about 0.5, indicating that these may be diffusion-controlled processes.

Bohm and Kahlweit (Ref 21) reported that the internal oxidation depth of Ni-Si alloys is ~18 μm after 63 h at 800 °C, corresponding to an oxygen diffusivity in a Ni-0.06Si alloy of 7.2×10^{-11} cm^2 s^{-1} and an oxygen solubility in Ni of 0.019 wt.% (Ref 22). The internal oxidation depth of the Ni-0.5Si alloy, measured by Barlow et al., was ~41 μm after 63 h at 900 °C under low oxygen partial pressure, where only silica formed (Ref 23). Compared to those data, the oxide thickness (and internal penetration) of the Ni_3Si alloys tested at much

lower temperatures (~165 °C) is much thicker, indicating that a different mechanism controls these processes in sulfuric acid.

3.2.3 Characterization of Oxide Film. The oxide layers of the corroded samples were removed by scraping the surfaces, then were ground to powders (<180 μm) and analyzed by XRD. Figure 7 shows the diffraction data from corroded samples of $NiSi_{20}Nb_3B_{0.5}$ in Stage II (2 h exposure) and Stage III (63 h exposure). The crystalline β-phase and the G-phase were identified, along with a broad peak associated with an amorphous phase (Fig. 7). The β-phase and G-phase were likely grains removed from the metal surface when the oxide layer was scraped away. Based on the position of the broad peak and the EDS results (Table 2), the amorphous phase most likely is SiO_2. Nickel sulfate hydrates ($NiSO_4{\cdot}(H_2O)$ and $NiSO_4{\cdot}6(H_2O)$) were found in the Stage II oxide layer, but not in the Stage III layer, consistent with the lower Ni content in the Stage III layer (Table 2). Similar results were noted for the oxide layers on the $NiSi_{21}Nb_{1.6}B_{0.5}$ coupons.

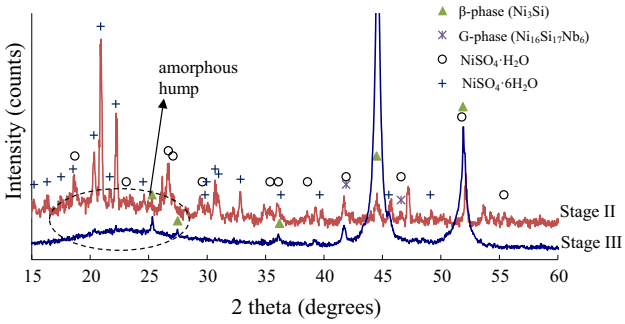

Fig. 7 XRD patterns of the oxide scale of $NiSi_{20}Nb_3B_{0.5}$ at Stage II (2 h exposure) and Stage III (63 h exposure) in boiling 70 wt.% sulfuric acid. At Stage III, there was almost no nickel sulfate hydrate in oxide scale

3.3 Effect of G-Phase ($Ni_{16}Si_{17}Nb_6$) on Corrosion

Like the α + β eutectic, the G-phase remains after the homogenization heat treatment (Ref 5), in the three alloys. The cross-sectional micrographs of corroded samples (Fig. 4) indicate that the G-phases were not selectively attacked by sulfuric acid. In fact, compositional depth profiles by Auger electron spectroscopy indicate that the G-phase oxidizes more slowly during Stage I than does the β-phase. Figure 8 shows depth profiles obtained through the oxide that formed on a G-phase grain (left) and on a β-phase grain (right) in a $NiSi_{20}Nb_3B_{0.5}$ sample exposed to boiling 70 wt.% sulfuric acid for 1 min; the silicon-rich oxide covering the G-phase was

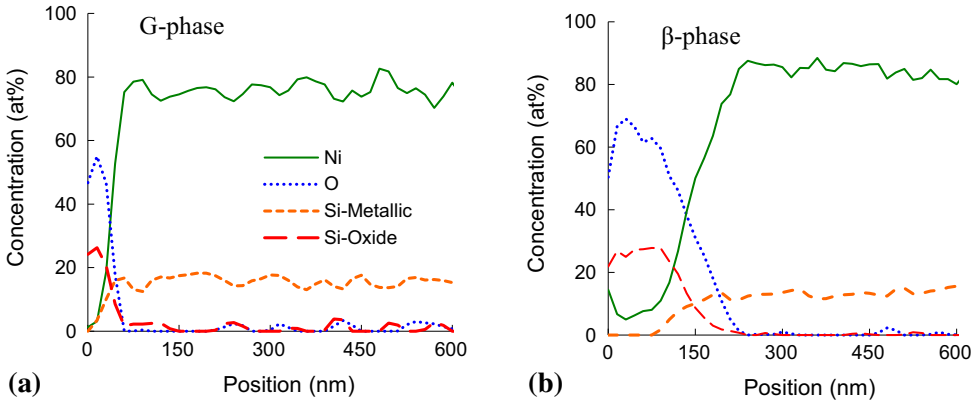

Fig. 8 Compositional depth profiles of the corroded (a) G-phase (b) β-phase of a $NiSi_{20}Nb_3B_{0.5}$ alloy exposed to boiling 70 wt.% sulfuric acid for 1 min. Compositions were obtained using scanning AES

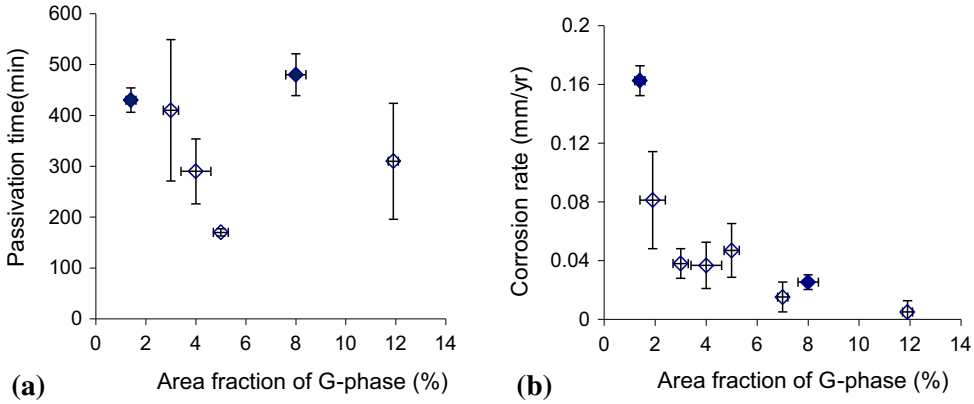

Fig. 9 The relationships between area fraction of the G-phase and (a) passivation time; (b) steady-state corrosion rate, for several $Ni_3(Si,Nb)$ alloys in boiling 70 wt.% sulfuric acid. Closed symbols are data from the present study and open symbols are from Ref 6 and 27

~50 nm thick and the oxide on the β-phase was ~220 nm thick. Zhang also reported that the G-phase acts as a cathode with the β-phase in conditions similar to those of this work (Ref 6). Generally, the two-phase alloys are less corrosion resistant than single phase alloys, owing to the electrochemical action between the two phases (Ref 24). But, in an environment where passivity is favored, the presence of a second phase that raises the initial current density might cause faster passivation (Ref 25). Since the protection of Ni_3Si alloys in the concentrated sulfuric acid is based on the formation of an oxide scale (Ref 15, 26), G-phase might have positive effects on the corrosion resistance of Ni_3Si alloys.

The area fraction of G-phase was determined by quantitative analyses of electron microscopy images and then related to the passivation time and the steady-state corrosion rate for the different $Ni_3(Si,Nb)$ alloys in boiling 70 wt.% sulfuric acid, as shown in Fig. 9(a) and (b), respectively. Included in these figures are data for different alloys corroded under the same conditions, as reported in Ref 6 and 27. The passivation time is independent of the G-phase content, but the steady-state corrosion rates seem to decrease with increasing G-phase fraction. The high steady-state corrosion rates of those samples with $<2\%$ G-phase might also be due to the corrosion of some residual $\alpha + \beta$ eutectic in matrix. The fraction of $\alpha + \beta$ eutectic in $Ni_3(Si,Nb)$ alloys with $>2\%$ G-phase is $<0.5\%$ (area fraction) and is ~1% in $Ni_3(Si,Nb)$ alloys with $<2\%$ G-phase.

4. Conclusions

Three $Ni_3(Si,Nb)$ alloys with different microstructures and phase combinations were tested in boiling 70 wt.% sulfuric acid and exhibited similar corrosion behavior, summarized by three distinct kinetic stages. Stage I was generally completed in less than 30 min. Most of the weight loss occurred over the next several hundred minutes in Stage II. During Stage III, the alloys passivated and the weight loss rate was the lowest.

An amorphous silica surface scale begins to form during Stage I and covers the entire surface in Stage II and Stage III. The thickness of the oxide scale follows parabolic kinetics through Stage II until passivation. Nickel sulfate hydrates can be detected in the Stage II oxide scales, but not in the Stage III scales.

The $\alpha(Ni) + \beta(Ni_3Si)$ eutectic is detrimental to corrosion resistance, as evidenced by internal penetration along this phase. On the other hand, the G-phase ($Ni_{16}Si_{17}Nb_6$), another major secondary phase in these microstructures, appears to oxidize more slowly than the β-matrix and contributes to a lower steady-state corrosion rate for the alloys.

Acknowledgements

The authors would like to thank Harry Meyer at Oak Ridge National Lab for his assistance with the Auger electron spectroscopy experiments, and Eric Bohannan at Missouri S&T for the XRD analyses. This work was supported by a NERI (National Energy Research Institute)-DOE (US Department of Energy) Project (DE-FC07-06ID14753).

Appendix

If one considers a typical thickness for the silica scale to be 30 microns (Fig. 6a), then using the density of amorphous silica (2.2 g cm^{-3}) and the relative weight fraction of oxygen atoms in silica, one calculates an increase in mass of approximately 0.004 g cm^{-2} to create the scale. The typical coupon weight loss over the same corrosion time is about five times as great, indicating that coupon dissolution has the greatest effect on the overall change in coupon mass. It is difficult to accurately measure the amount of nickel sulfates in surface scale. But, based on the similar estimation, the weight change caused by the small amount of nickel sulfates (Table 2) is not critical.

References

1. S. Kubo, H. Nakajima, S. Kasahara, S. Higashi, T. Masaki, H. Abe, and K. Onuki, A Demonstration Study on a Closed-Cycle Hydrogen Production by the Thermochemical Water-Splitting Iodine-Sulfur Process, *Nucl. Eng. Des.*, 2004, **233**, p 347–354
2. L.C. Brown, G.E. Besenbruch, R.D. Lentsch, K.R. Schultz, J.F. Funk, and P.S. Pickard, High Efficiency Generation of Hydrogen Fuels Using Nuclear Power, General Atomics Report GA-A24285 Rev 1, 2003
3. A.M. Russell, Ductility in Intermetallic Compounds, *Adv. Eng. Mater.*, 2003, **5**, p 629–639
4. D.W. Wakeman, F.G. Haines, K.J. Williams, T.J. Evans, and W. Barker, Nickel-Silicon Alloys, U.K. Patent 1041484-A, 1966
5. J.W. Newkirk, J.-H. Hsu, R.K. Brow, and T. Lillo, Chromium-Free Nickel Alloys for Hot Sulfuric and Sulfur Environments, *Int. J. Hydrogen Energy*, 2011, **36**, p 4588–4594
6. S.-H. Zhang, The Development of Nickel Silicide Based Alloy for Sulfuric Acid Application, A Dissertation in Metallurgical Engineering of University of Missouri Rolla, 2000
7. W. Barker, T.E. Evans, and K.J. Williams, Effects of Alloying Additions on the Microstructure, Corrosion Resistance and Mechanical Properties of Nickel-Silicon Alloys, *Br. Corros. J.*, 1970, **5**, p 76–86
8. P. Kumar, High-Temperature Ordered Intermetallic Alloys, *Mat. Res. Soc. Symp. Proc.*, 1980, **39**, p 537–554
9. T. Takasugi and M. Yoshida, Mechanical Properties of the $Ni_3(Si, Ti)$ Alloys Doped with Carbon and Beryllium, *J. Mater. Sci.*, 1991, **26**, p 3032–3040
10. C.M. Larson, The Corrosion of Nickel-Silicon Based Alloys in Sulfuric Acid, a Thesis in Material Science and Engineering of Missouri S&T, 2008
11. F.X. Spiegel, D. Bardos, and P.A. Beck, Ternary G and E Silicides and Germanides of Transition Elements, *Trans. Metall. Soc. AIME*, 1963, **227**, p 575–579
12. J.W. Newkirk and S.-H. Zhang, Corrosion Resistant Nickel-Based Alloy, U.S. Patent 6342181, 2002
13. M. Davies, *Materials Selection for Sulfuric Acid*, 2nd ed., Materials Technology Institute, St. Louis, 2005
14. G. Kreysa and M. Schitze, *Corrosion Handbook: Corrosive Agents and Their Interaction with Materials. Volume 11: Sulfuric Acid*, 2nd ed., Wiley, New York, 2008
15. T.E. Evans and A.C. Hart, Corrosion and Passivation of a Nickel-Silicon Base Alloy in Sulfuric Acid Solutions, *Electrochim. Acta*, 1970, **16**, p 1955–1970
16. C.T. Liu, E.P. George, and W.C. Oliver, Grain-Boundary Fracture and Boron Effect in Ni_3Si Alloys, *Intermetallics*, 1996, **4**, p 77–83
17. Standard Practice for Laboratory Immersion Corrosion Testing of Metals, G31–72, American Society for Testing and Materials, 2004
18. W.W. Duecher and J.R. West, *The Manufacture of Sulfuric Acid*, Reinhold, New York, 1959
19. G. Priyotomo, S. Wagle, K. Okitsu, A. Iwase, Y. Kaneno, R. Nishimura, and T. Takasugi, The Corrosion Behavior of Ni3(Si, Ti) Intermetallic Compounds with Al, Cr, and Mo in Various Acidic Solutions, *Corros. Sci.*, 2012, **60**, p 10–17

20. R. Matsuhashi, H. Abo, S. Abe, and Hiroshi Kihira, Corrosion Mechanism of Stainless Steels in Highly Concentrated Sulfuric Acid, *Corros. Eng.*, 1987, **36**, p 578–585
21. G. Bohm and M. Kahlweit, On Internal Oxidation of Metallic Alloys, *Acta Met.*, 1964, **12**, p 641–648
22. E.A. Brandes, *Smithells Metals Reference Book*, 6th ed., Butterworths, Boston, 1983
23. R. Barlow and P.J. Grundy, The Determination of the Diffusion Constants of Oxygen in Nickel and α-Iron by an Internal Oxidation Method, *J. Mater. Sci.*, 1969, **4**, p 797–801
24. D.A. Jones, *Principles and Prevention of Corrosion*, 2nd ed., Prentice-Hall, New Jersey, 1996
25. U.R. Evans, *Metallic Corrosion Passivity and Protection*, Edward Arnold & Co., London, 1937
26. J.H. Chang, J.M. Chou, R.I. Hsieh, and J.L. Lee, Corrosion Behaviour of Vacuum Induction-Melted Ni-Based Alloy in Sulphuric Acid, *Corros. Sci.*, 2010, **52**, p 2323–2330
27. J.-H. Hsu, Understanding Corrosion of Ni_3(Si,Nb) Alloys in Hot Sulfuric Acid, a Dissertation in Metallurgical Engineering of Missouri S&T, 2010